ASTRONOMY & ASTROPHYSICS
SUPPLEMENT SERIES

Astron. Astrophys. Suppl. Ser. **137**, 505–519 (1999)

Spectroscopy of the post-AGB star HD 101584 (IRAS 11385 − 5517)⋆

T. Sivarani[1], M. Parthasarathy[1], P. García-Lario[2], A. Manchado[3], and S.R. Pottasch[4]

[1] Indian Institute of Astrophysics, Bangalore 560 034, India
[2] ISO Data Centre, Astrophysics Division, Space Science Department of ESA, Villafranca del Castillo, Apartado de Correos 50727, E-28080 Madrid, Spain
[3] Instituto de Astrofisica de Canarias, E-38200 La Laguna, Tenerife, Spain
[4] Kapteyn Astronomical Institute, Postbus 800, NL-9700 AV Groningen, The Netherlands

Received October 22, 1998; accepted May 12, 1999

Abstract. From an analysis of the spectrum (4000 Å to 8800 Å) of HD 101584 it is found that most of the neutral and single ionized metallic lines are in emission. The forbidden emission lines of [OI] 6300 Å and 6363 Å and [CI] 8727 Å are detected, which indicate the presence of a very low excitation nebula. The Hα, FeII 6383 Å, NaI D_1, D_2 lines and the CaII IR triplet lines show P-Cygni profiles indicating a mass outflow. The Hα line shows many velocity components in the profile. The FeII 6383 Å also has almost the same line profile as the Hα line indicating that they are formed in the same region. From the spectrum synthesis analysis we find the atmospheric parameters to be $T_{\rm eff}$ = 8500 K, log g = 1.5, $V_{\rm turb}$ = 13 km s^{-1} and [Fe/H] = 0.0. From an analysis of the absorption lines the photospheric abundances of some of the elements are derived. Carbon and nitrogen are found to be overabundant. From the analysis of Fe emission lines we derived $T_{\rm exi} = 6100$ K ± 200 for the emission line region.

Key words: stars: abundances-stars: evolution-stars: post-AGB-stars: circumstellar matter-stars: individual: HD 101584

1. Introduction

Humphreys & Ney (1974) found near-infrared excess in HD 101584 and suggested that it is a massive F-supergiant with an M-type binary companion star (Humphreys 1976). However, HD 101584 (V = 7.01, F0 Iape (Hoffleit et al. 1983) was found to be an IRAS source (IRAS 11385−5517) (Parthasarathy & Pottasch 1986). On the basis of its far-infrared colors, flux distribution and detached cold circumstellar dust shell, Parthasarathy & Pottasch (1986) suggested that it is a low mass star in the post-Asymptotic Giant Branch (post-AGB) stage of evolution.

CO molecular emission lines at millimeter wavelengths were detected by Trams et al. (1990). The complex structure of the CO emission shows large Doppler velocities of 130 km s^{-1} with respect to the central velocity of the feature indicating a very high outflow velocity. Te Lintel Hekkert et al. (1992) reported the discovery of OH 1667 MHz maser emission from the circumstellar envelope of HD 101584. The OH spectrum has a velocity range of 84 km s^{-1} and shows two unusually broad emission features. Te Lintel Hekkert et al. (1992) found from the images obtained from the Australian Telescope, that the OH masers are located along the bipolar outflow. The post-AGB nature of HD 101584 is also suggested by the space velocity of the star derived from the central velocity of the CO and OH line emission. This velocity of $V_{\rm rad}$ = 50.3 ± 2.0 km s^{-1} does not agree with the galactic rotation curve assuming it to be a luminous massive population I F supergiant.

Bakker et al. (1996a) studied the low and high resolution ultraviolet spectra and the high resolution optical spectra of HD 101584. Based on the strength of HeI (see also Morrison & Zimba 1989) N II, C II lines and Geneva photometry, Bakker et al. (1996a) suggest that HD 101584 is a B9 II star of $T_{\rm eff}$ = 12000 K ± 1000 K and log g = 3.0. Bakker et al. (1996b) also found small amplitude light and velocity variations and suggested that HD 101584 is a binary with an orbital period of 218 days.

Send offprint requests to: T. Sivarani

⋆ Based on observations obtained at the European Southern Observatory (ESO), Chile and the Vainu Bappu Observatory, Kavalur, India.

Correspondence to: sivarani@iiap.ernet.in

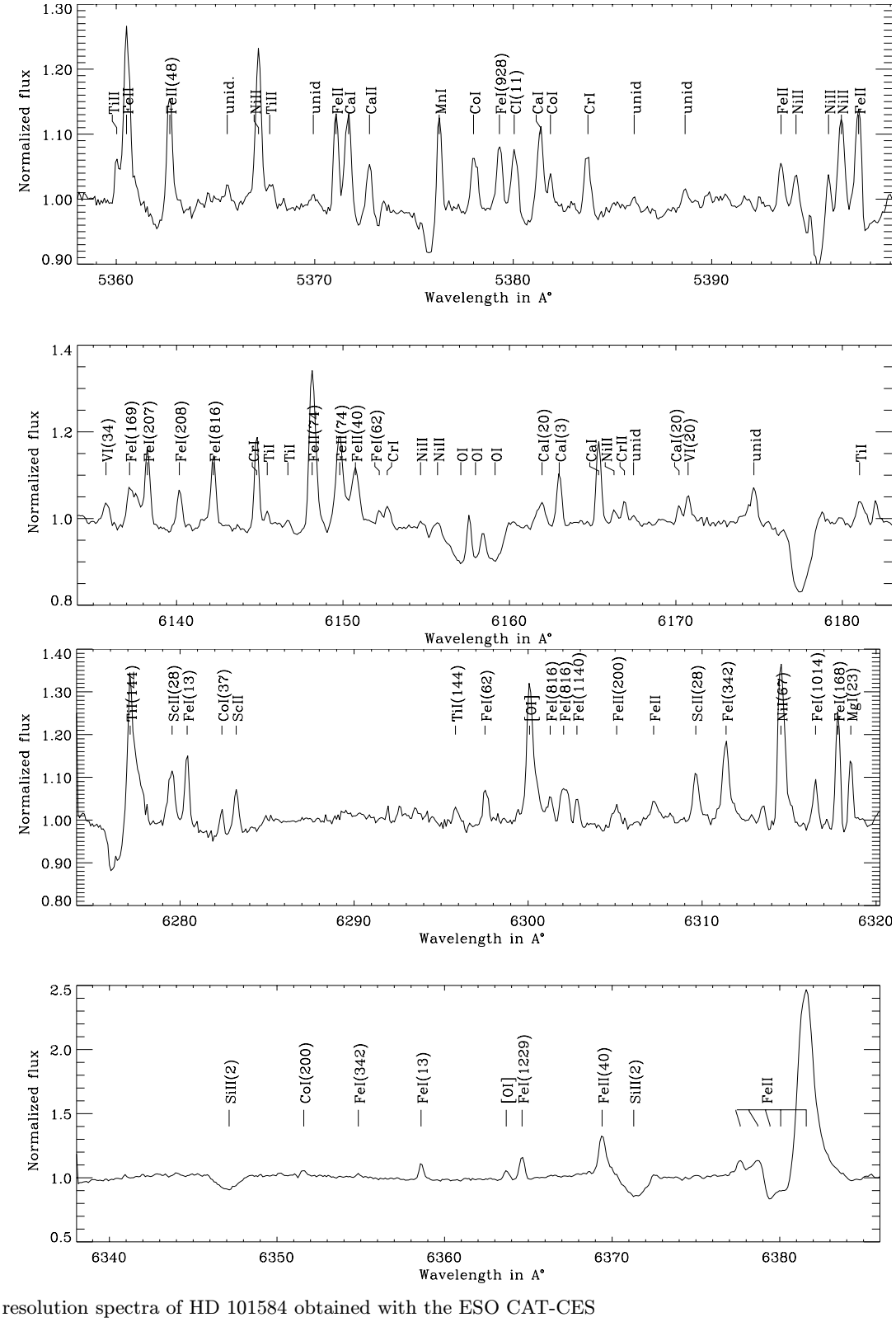

Fig. 1. High resolution spectra of HD 101584 obtained with the ESO CAT-CES

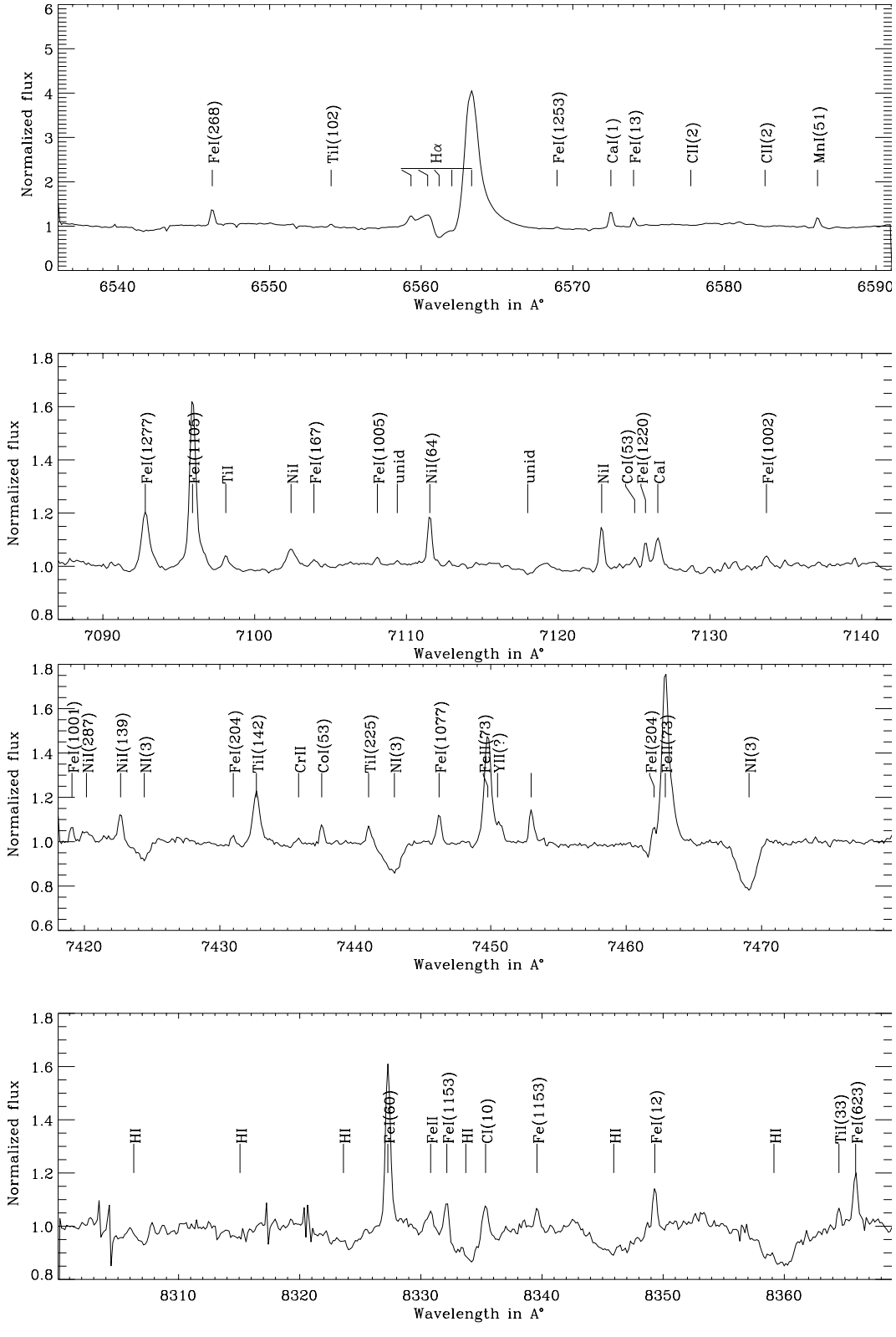

Fig. 1. continued

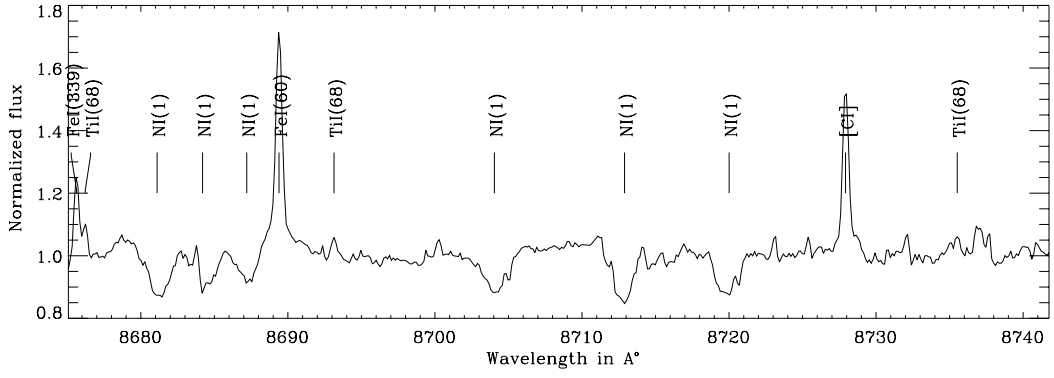

Fig. 1. continued

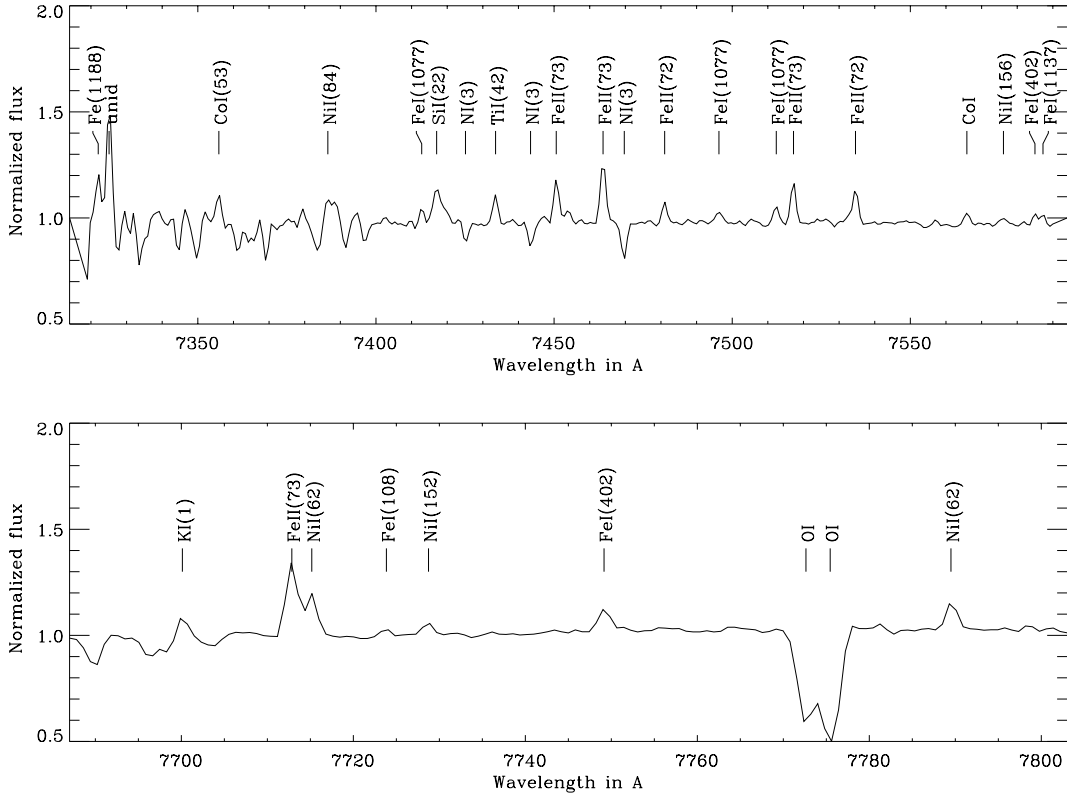

Fig. 2. The spectrum in the upper panel shows several nitrogen lines and emission lines of Fe. The lower panel shows the KI 7699 Å in emission and the strong absorption due to OI triplet at 7777 Å

The optical spectrum of HD 101584 is very complex and shows many lines in emission. In this paper we report an analysis of the high resolution optical spectrum of HD 101584.

2. Observations and analysis

High resolution and high signal to noise ratio spectra of HD 101584 were obtained with the European Southern Observatory (ESO) Coude Auxiliary Telescope (CAT) equipped with the Coude Echelle Spectrograph (CES) and a CCD as detector. The spectra cover the wavelength regions 5360 − 5400 Å, 6135 − 6185 Å, 6280 − 6320 Å, 6340−6385 Å, 6540−6590 Å, 7090−7140 Å, 7420−7480 Å, 8305 − 8365 Å and 8680 − 8740 Å. The spectral resolution ranged from 0.165 Å at 6150 Å to 0.210 Å at 8700 Å. We have also obtained 2.5 Å resolution spectra of HD 101584 from 3900 Å to 8600 Å with the 1 m telescope and UAGS spectrograph and a CCD as detector at the Vainu Bappu Observatory (VBO), Kavalur, India. In addition we obtained CCD spectra with the same telescope and Coude Echelle spectrograph, covering the wavelength region 4600 Å to 6600 Å with a resolution of 0.4 Å. All spectra mentioned above were used in this analysis.

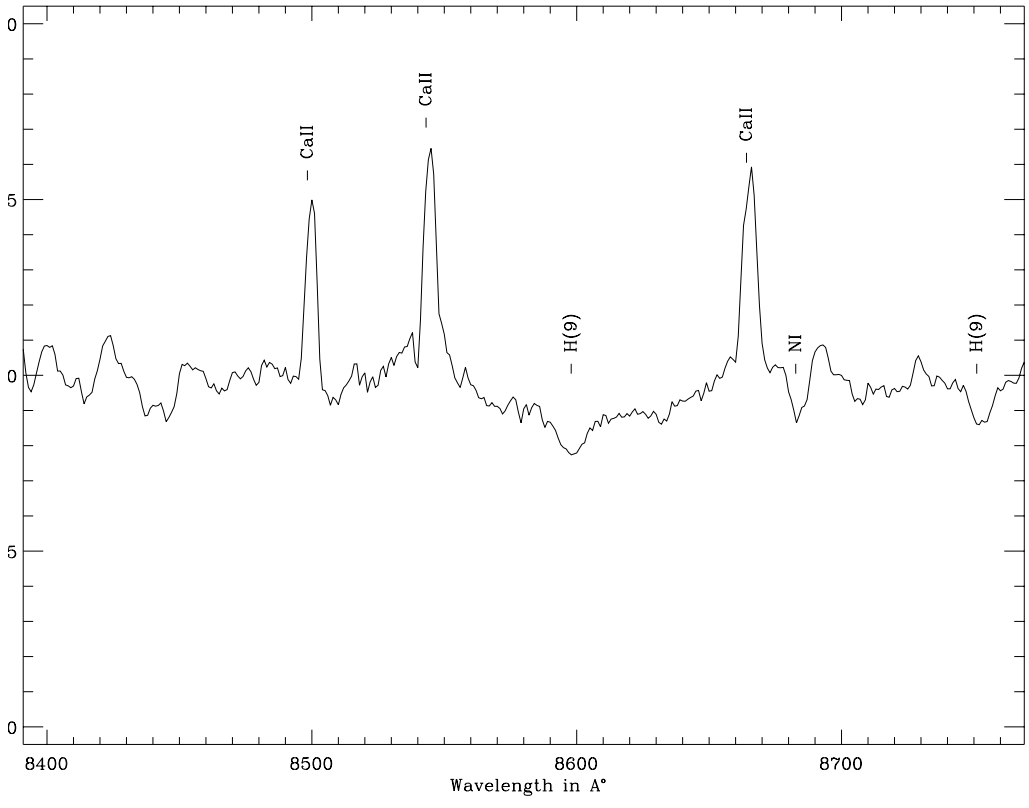

Fig. 3. CaII IR triplet lines showing P-Cygni emission.This spectrum is of 2.5 Å resolution, obtained from VBO, Kavalur

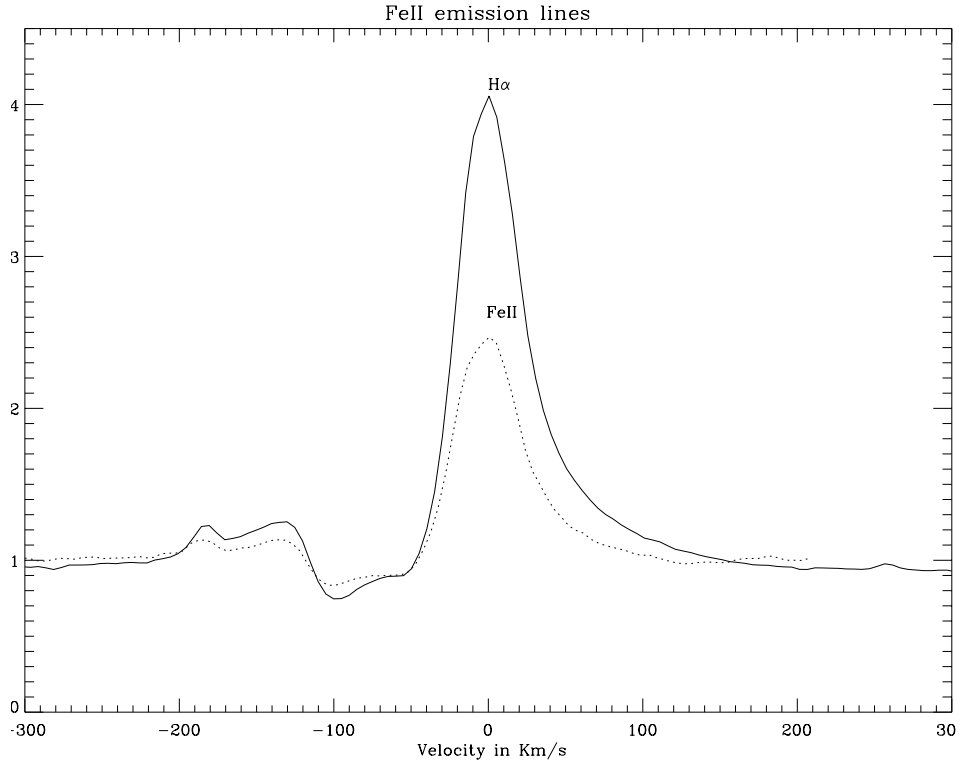

Fig. 4. P-Cygni profile of Hα and FeII(6383 Å) lines showing similar velocity structures

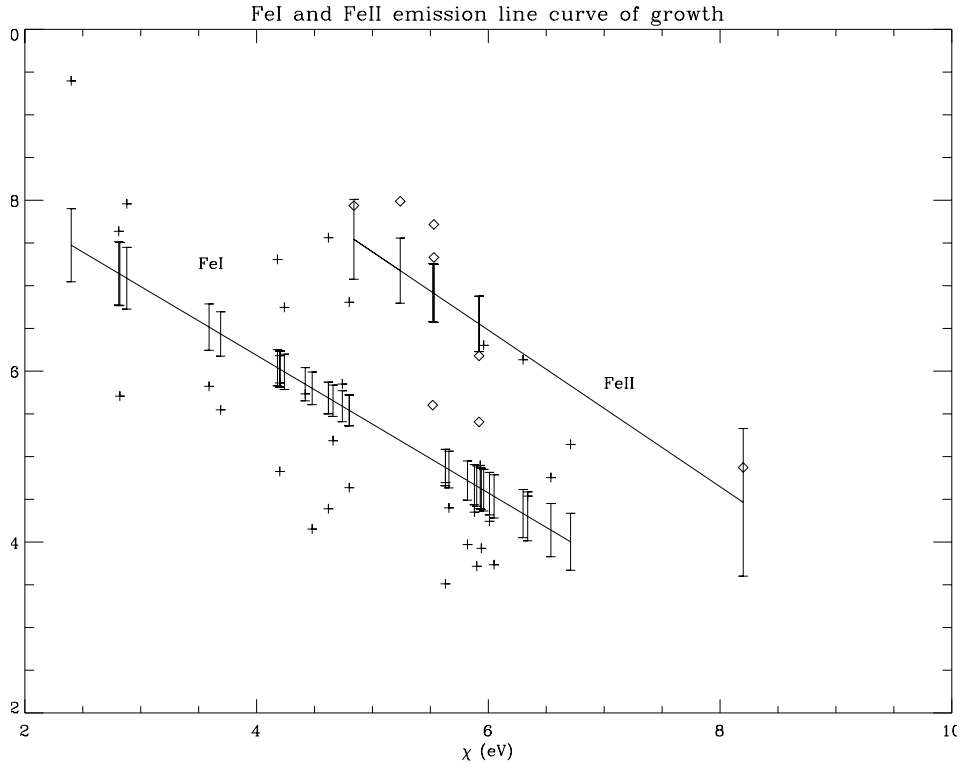

Fig. 5. Curve of growth analysis of Fe emission lines. + represents the FeI lines and ♢ represents FeII lines. The slope gives $T_{\rm exi} = 6300 \pm 1000$ K for FeI lines and $T_{\rm exi} = 5550 \pm 1700$ K for the FeII lines. The large dispersion is because the lines are optically thick. The errors bar show the error in the least square fit

All the spectra were analyzed using IRAF software. The equivalent widths of lines were found by fitting a Gaussian. For blended lines de-blending was done by fitting multiple Gaussians. We carried out spectrum synthesis calculations using KURUCZ stellar models (1994). SYNSPEC code (Hubeny et al. 1985) was used for calculating the theoretical line profiles. The gf values were taken from Wiese et al. (1966), Wiese & Martin (1980), Hibbert et al. (1991), Parthasarathy et al. (1992) and Reddy et al. (1997 and references therein). For the analysis of forbidden lines we have used the IRAF software package NEBULAR under STSDAS.

3. Description of the spectrum

The remarkable characteristic of the optical spectrum of HD 101584 is the fact that different spectral regions resemble different spectral types. The spectrum in the UV region is similar to that of α Lep which is an F-supergiant (Bakker 1994). The optical spectrum in the range 3600 Å − 5400 Å is dominated by absorption lines. Most of them are due to neutral and single ionized lines of Ti, Cr and Fe. The CaII H and K absorption lines are strong. The strength of the absorption lines are similar to that observed in an A2 supergiant. In the yellow and red spectral regions, most of the lines are in emission (Fig. 1). The emission lines show complex line profiles. The absorption lines of NI, OI, CII and SiII are broad. The Paschen lines are in absorption. Some of these absorption lines are blended with emission lines and many have asymmetric profiles. The OI lines at 6156 Å are blended with emission lines of FeI. The NI lines are strong and show asymmetric line profiles. The blue wing is shallow compared to the red wing. The CII lines at 6578 Å and 6582 Å are weak. The Na D lines, KI 7700 Å (Fig. 2), the CaII IR triplet lines (Fig. 3), [OI], [CI] and MgI 6318.7 Å lines are found in emission. The OI triplet lines (Fig. 2) are very strong indicating an extended atmosphere and NLTE effects.

3.1. P-Cygni profiles

The Hα line has a very strong P-Cygni profile indicating an outflow. The profile looks very complex. It shows at least 6 velocity components. The FeII line at 6383 Å is in emission and the profile is very similar to that of Hα (Fig. 4). Similar behaviour of the 6383 Å FeII line and Hα line is also noticed in the post-AGB F supergiant IRAS 10215 − 5916 (García-Lario et al. 1994). The Hα and the FeII 6383 Å line show an outflow velocity of 100 ± 10 km s^{-1}. The Hβ line also shows a P-Cygni profile. It has a broad emission wing at the red end. This indicates that the line forming region is extended. The Hβ,

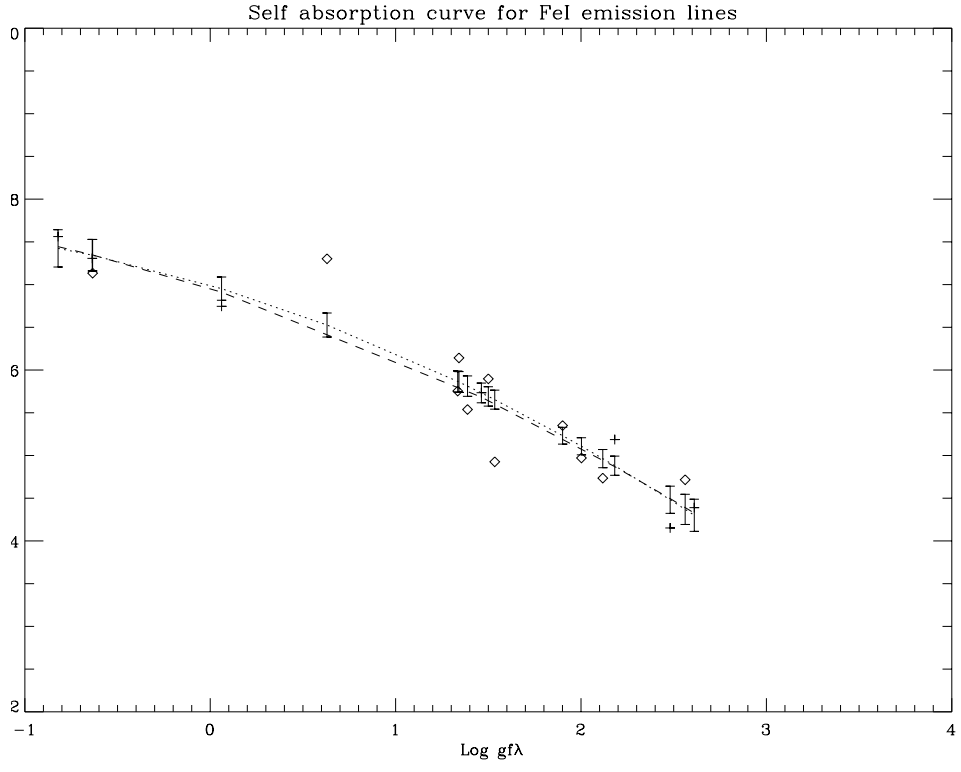

Fig. 6. a) The plot shows the shape of the SAC. The + sign indicates multiplets 167, 168, 169, 204, 207, 208 of Fe I having similar excitation potential. ◇ indicates multiplets 1002, 1005, 1014, 1077, 1105, 1140, 1153, 1220, 1229, 1277 of FeI. The fit was obtained after shifting higher multiplets 1002, 1005, 1014, 1077, 1105, 1140, 1153, 1220, 1229, 1277 w.r. to the lower multiplets 167, 168, 169, 204, 207, 208

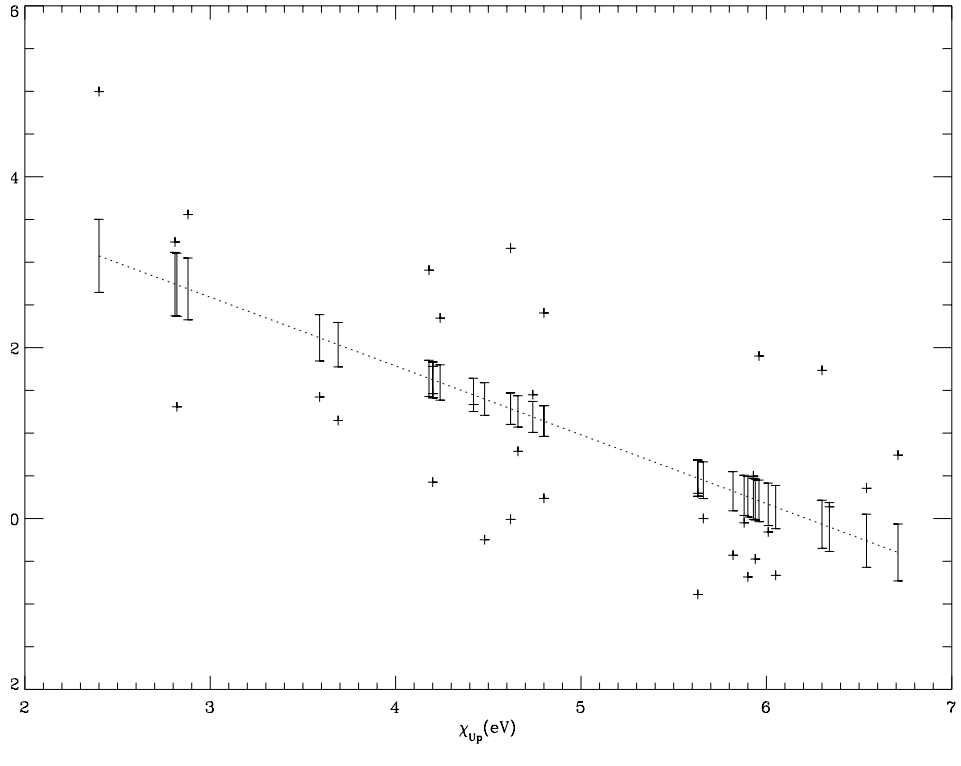

Fig. 6. b) The fit shows the distribution of upper level population of different multiplets of FeI with respect to the multiplet 207, versus the upper excitation potential

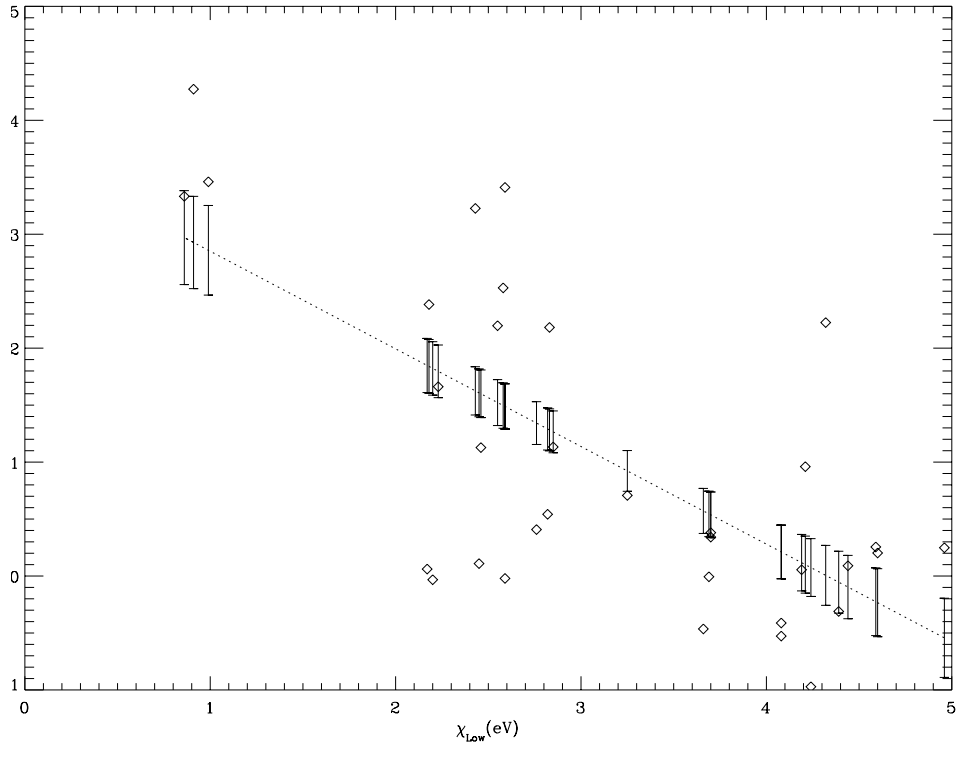

Fig. 6. c) The fit shows the distribution of lower level population of different multiplets of FeI with respect to the multiplet 207, versus the lower excitation potential

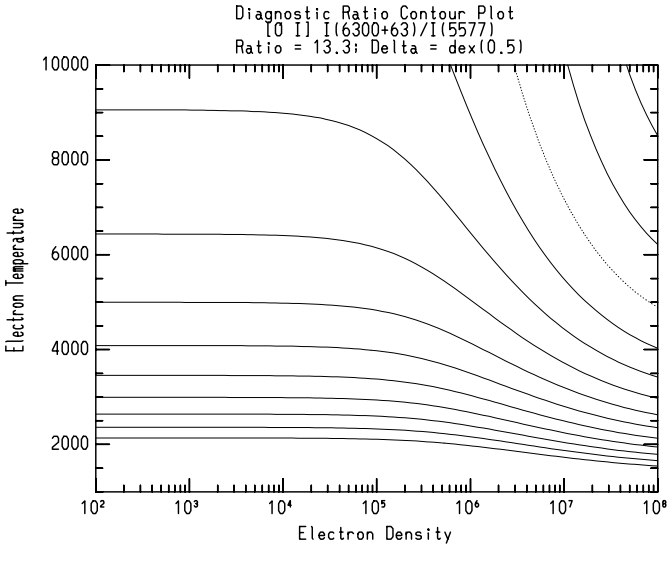

Fig. 7. Plot of electron density N_e and electron temperature T_e. The dotted line is the contour for the observed ratio (13.3) of [O]I lines 5577 Å, 6300 Å and 6363 Å. Each contour in the plot is for a change in the flux ratio of 0.5

NaI D1, D2 and the CaII IR triplet lines (Fig. 3) show an outflow velocity of 75 ± 20 km s^{-1}. The velocity structure seen in these P-Cygni profiles could be due to emission from different shells formed during the episodic mass-loss events.

3.2. FeI and FeII emission lines

The presence of numerous emission lines of FeI and FeII makes it possible to derive the physical conditions of the line forming region. From the curve of growth analysis of the FeI and FeII emission lines (Viotti 1969), we have derived $T_{\rm exi} = 6300 \pm 1000$ K and 5550 ± 1700 K respectively (Fig. 5). The scatter found could be due to the fact that the lines are not optically thin. On the other hand, there are only few emission lines of FeII present in the spectra and thus the estimate from FeII might not be accurate. In order to determine whether the large scatter observed in Fig. 4 is reflecting optical thickness effects we have done self-absorption curve (SAC) analysis (Friedjung & Muratorio 1987) for the FeI emission lines.

SAC is a kind of curve of growth applied to emission lines, but it has certain advantages as compared to the classical emission line curve of growth analysis. This method of analysis is valid also for optically thick lines. It deals with each transition separately, so that it is possible to get the population of different levels without assuming a Boltzmann distribution. In this curve, a function of the line flux emitted in the different transition of a given multiplet is taken in such a way that it is constant for a optically thin uniform medium. As the optical thickness increases the curve will move towards a straight line inclined at $-45^{\rm o}$. The shape of the SAC in Fig. 6a shows the lines are optically thick. The shape of the SAC is obtained

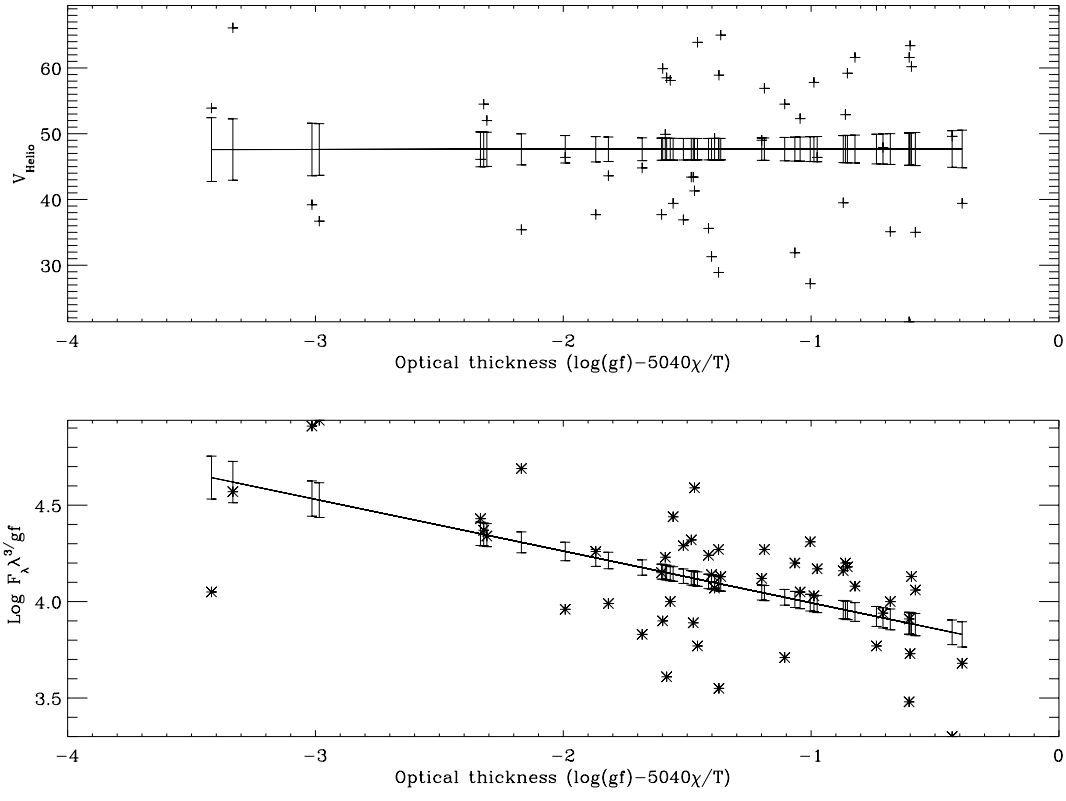

Fig. 8. The plot in the upper panel does not show any correlation between the optical depth and the helio centric radial velocity for the FeI absorption lines of HD 101584 in the wavelength region 3600 Å − 4500 Å. The plot in the lower panel shows the normalized strength of FeI absorption lines in the wavelength region 3600 Å to 4500 Å versus the optical depth. It shows clearly that the lines are forming at different optical depths. The equivalent widths are taken from the paper by Rosenzweig et al. (1997)

by shifting all the multiplets with respect to a reference multiplet. Here we have taken multiplet 207 as reference. The X and Y shifts of each multiplet gives the relative population of the lower and upper level with respect to the reference multiplet. Figures 6b,c shows the Y and X shifts versus the upper and lower excitation potential from which we derive the $T_{\rm exi} = 6100 \pm 200$ K.

3.3. Forbidden lines

The forbidden emission lines at 5577 Å, 6300 Å and 6363 Å of neutral oxygen are present in the spectra. The forbidden line of neutral carbon at 8727 Å is also seen. The 6300 Å line is blended with ScII line and the 5577 Å line is very weak. We have calculated the $I(6300)+I(6363)/I(5577)$ to be 13.3. From the flux ratio we can calculate $T_{\rm e}$ (Osterbrock 1989). This flux ratio is not very accurate because of very the weak 5577 Å line and poor signal to noise spectrum. For the flux ratio of 13.3 we derived a function depending on the electron density $N_{\rm e}$ and temperature $T_{\rm e}$. Figure 7 shows the $N_{\rm e}$ and $T_{\rm e}$ contours for different values of flux ratio around 13.3. Since we do not see any other forbidden lines which are sensitive to the electron density, we could not fix both $N_{\rm e}$ and $T_{\rm e}$ uniquely. But assuming a temperature derived from the Fe emission lines, an electron density of 1 10^7 is obtained. For this value of electron density and temperature the C/O = 0.5 ± 0.2 has been obtained.

4. Radial velocities

There are very few absorption lines and most of these are affected by emission and or a shell component, therefore we derived the average radial velocity from the well defined emission lines. The average radial velocity from the emission lines is found to be 50 ± 2 km s^{-1}. Morrison & Zimba (1989) using 14 best absorption lines found the radial velocity to be 69 ± 1 km s^{-1}. From the equivalent widths of FeI absorption lines given by Rosenzweig et al. (1997) we find no correlation between log $gf - \chi\Theta$ and heliocentric radial velocity (Fig. 8). However, Bakker et al. (1996a) found a correlations between log $gf - \chi\Theta$ and heliocentric radial velocities of HD 101584 in the UV. The discripancy could be due to the poor resolution of Rosenzweig et al. (1997) data compared to that of Bakker et al. (1996a). The large scatter seen in the radial velocities could be due to pulsation. Similar velocity variations

Table 1. List of emission lines detected in the high resolution spectrum of HD 101584

λ obs (Å)	λ lab (Å)	Ident.	χ (eV)	log gf	$F_\lambda{}^*$ (mÅ)	$\Delta\lambda$ (Å)	$V_{\rm Helio}$ km s^{-1}
5360.022	5360.115	TiII	2.60−4.92	−4.040		−0.093	10.60
5360.517	5360.755	FeII	10.52−12.83	−3.082	118.4	−0.237	2.51
5362.698	5362.864	FeII(48)	3.20−5.52	−2.739	47.36	−0.165	6.56
5365.597		unid					
5367.167	5367.205	NiII	14.61−16.93	−2.571	79.71	−0.038	13.69
5367.731	5367.912	TiII	1.57−3.88	−4.480		−0.181	5.69
5369.928	5369.928	unid					
5371.07	5371.275	FeII	10.56−12.87	−0.705	45.52	−0.20	4.36
5371.704	5371.934	CaI	5.4−7.71	−3.163		−0.220	2.97
5372.76	5372.807	CaII	9.03−11.35	−1.337	21.64	−0.04	13.17
5376.27	5376.477	MnI	2.93−5.23	−4.091	45.13	−0.20	4.26
5378.	5378.247	CoI	4.03−6.34	−0.425	32.41	−0.24	2.03
5379.305	5379.581	FeI(928)	3.70−6.01	−1.521	33.83	−0.275	0.43
5380.048	5380.322	CI(11)	7.70−10.00	−1.840	32.67	−0.273	0.54
5381.379	5381.599	CaI	5.46−7.77	−4.960	49.97	−0.220	3.54
5381.874	5382.046	CoI	4.51−6.82	−3.234	15.82	−0.171	6.24
5383.763	5383.927	CrI	4.54−6.85	−2.606	22.12	−0.163	6.70
5386.093	5386.093	unid					
5388.659	5388.659	unid					
5393.491	5393.762	FeII	11.19−13.49	−2.154	17.12	−0.270	0.74
5394.247	5394.496	NiII	12.64−14.94	−1.029	14.61	−0.249	1.97
5395.886	5396.051	NiII	14.63−16.93	−2.851	10.14	−0.164	6.67
5396.532	5396.701	NiII	14.63−16.93	−2.561	54.78	−0.168	6.42
5397.4	5397.640	FeII	10.73−13.03	−2.883	51.29	−0.240	2.46
6133.723	7132.985	FeI(1002)	4.08−5.82	−0.851	36.31	0.738	46.96
6135.76	6135.370	VI(34)	1.05−3.08	−0.750	23.13	0.389	35.22
6137.179	6136.624	FeI(169)	2.45−4.48	−1.307	30.29	0.555	43.31
6138.25	6137.702	FeI(207)	2.59−4.62	−1.177	70.63	0.547	42.95
6140.167	6139.65	FeI(208)	2.59−4.62	−4.609	38.79	0.517	41.43
6142.214	6141.727	FeI(816)	3.70−5.63	−1.540	61.82	0.486	39.95
6154.659	6154.094	NiII	14.88−16.91	−2.268	5.54	0.564	43.71
6144.813	6144.294	CrI	4.10−6.13	−3.624	80.21	0.519	41.51
6145.448	6144.936	TiI	1.89−3.91	−2.520	16.08	0.512	41.17
6146.688	6146.27	TiI(153)	3.18−5.20	−2.541	15.79	0.417	36.57
6148.146	6147.742	FeII(74)	3.89−5.92	−2.721	20.85	0.403	35.87
6149.804	6149.249	FeII(74)	3.89−5.92	−2.724	122.7	0.555	43.25
6150.747	6150.10	FeII(40)	3.22−5.24	−4.754	73.71	0.646	47.73
6152.178	6151.624	FeI(62)	2.18−4.20	−3.582	17.06	0.554	43.20
6152.655	6152.098	CrI	4.10−6.12	−1.986	33.16	0.556	43.31
6155.679	6155.102	NiII	13.14−15.16	−0.682	7.19	0.577	44.30
6161.957	6161.295	CaI(20)	2.53−4.54	−1.293	27.97	0.662	48.41
6162.99	6162.180	CaI(3)	1.90−3.92	−0.167	49.42	0.810	55.61
6165.354	6164.716	CaI	6.05−8.07	−2.261	73.94	0.638	47.22
6166.282	6165.893	NiII	9.75−11.77	−2.297	9.67	0.389	35.10
6166.907	6166.187	CrII	13.06−15.07	−3.490	18.24	0.720	51.21
6167.456	6167.456	unid			10.3		
6170.189	6169.559	CaI(20)	2.53−4.54	−0.527	13.17	0.629	46.80
6170.733	6170.340	VI(20)	4.80−6.81	−0.654	23.53	0.216	26.71
6174.685	6174.685	unid			39.17		
6181.032	6180.625	TiI	3.18−5.19	−3.632	43.54	0.407	35.93
6277.13	6277.470	TiI(144)	1.73−3.71	−3.794	112.2	−0.205	6.20
6279.541	6279.740	ScII(28)	1.5−3.48	−1.265	41.49	−0.287	2.29
6280.406	6280.622	FeI(13)	0.86−2.83	−3.720	44.44	−0.216	5.67
6282.404	6282.638	CoI(37)	1.74−3.72	−2.021	13.03	−0.234	4.81

Table 1. continued

λ obs (Å)	λ lab (Å)	ID	χ (eV)	log gf	$F_\lambda{}^*$ (mÅ)	$\Delta\lambda$ (Å)	$V_{\rm Helio}$ km s^{-1}
6283.225	6283.353	ScII	7.45−9.43	−0.441	40.34	−0.127	9.90
6295.826	6295.949	TiI(144)					
6297.524	6297.799	FeI(62)	2.23−4.20	−2.871	39.23	−0.274	2.91
6300.083	6300.311	[OI]			163	−0.228	5.15
6301.27	6301.508	FeI(816)	3.66−5.63	−0.745	23.32	−0.237	4.68
6302.042	6302.499	FeI(816)	3.69−5.66	−1.203	62.88	−0.457	−5.75
6302.807	6303.461	FeI(1140)	4.32−6.30	−3.434	20.01	−0.653	−15.11
6305.09	6305.314	FeII(200)	6.23−8.20	−2.039	27.17	−0.224	5.34
6307.214	6307.529	FeII	2.83−4.80	−5.685	57.4	−0.314	1.02
6309.636	6309.886	ScII(28)	1.5−3.47	−1.630	55.71	−0.250	4.12
6311.379	6311.504	FeI(342)	2.83−4.80	−3.392	103.2	−0.125	10.06
6313.52							
6314.529	6314.668	NiI(67)	4.16−6.13	−0.921	163.5	−0.139	9.39
6316.52	6315.814	FeI(1014)	4.08−6.05	−0.683	44.72	0.706	49.54
6317.802	6318.027	FeI(168)	2.46−4.42	−2.338	98.8	−0.181	7.40
6318.545	6318.717	MgI(23)	5.12−7.08	−1.730	60.1	−0.171	7.84
6351.598	6351.448	CoI(200)					
6354.852	6355.027	FeI(342)	2.85−4.80	−2.346	7.6	−0.174	7.62
6358.596	6358.687	FeI(13)	0.86−2.81	−4.546	47.9	−0.0908	11.59
6363.68	6363.79	[OI]			28.9	−0.109	10.69
6364.625	6364.706	FeI(1229)	4.59−6.54	−1.469	74.78	−0.081	12.05
6369.4	6369.464	FeII(40)	2.89−4.84	−4.253	186.8	−0.063	12.86
6380.058	6383.715	FeII	5.56−7.50	−2.271	1512	−3.656	−155.97
6381.582	6381.416	TiI(196)					
6539.783	6539.72	FeI(405)					
6546.217	6546.245	FeI(268)	2.76−4.66	−1.634	127.2	−0.0283	14.97
6554.056	6554.226	TiI(102)	1.44−3.34	−1.201	32.48	−0.169	8.49
6561.179	6561.179	Hα			3681		
6563.326	6563.403	CoI(80)					
6568.959	6569.231	FeI(1253)					
6572.512	6572.779	CaI(1)	0.00−1.89	−4.104	124.5	−0.266	4.10
6574.009	6574.238	FeI(13)	0.99−2.88	−4.688	65.55	−0.229	5.82
6574.831	6575.022	FeI(207)					
6580.992	6581.220	FeI(34)					
6586.144	6586.343	MnI(51)					
6587.438	6587.75	CI(22)					
7092.793	7091.942	FeI(1277)	4.96−6.71	−1.509	120.4	0.886	53.22
7095.905	7095.425	FeI(1105)	4.21−5.96	−2.221	337.4	0.479	36.21
7098.1	7097.655	TiI	3.30−5.30	−3.423	16.88	0.445	34.74
7102.397	7101.932	NiI	4.54−6.29	−1.941	53.25	0.464	35.55
7103.904	7103.15	FeI(167)	2.43−4.18	−4.488	18.39		
7108.084	7107.468	FeI(1005)	4.19−5.94	−1.317	11.32	0.449	34.87
7109.397	7109.397	unid			8.62		
7111.541	7110.905	NiI(64)	1.93−3.68	−3.042	70.85	0.648	43.29
7117.991	7117.991	unid			23.54		
7122.867	7122.191	NiI(126)	3.54−5.29	−0.169	55.08	0.676	44.40
7125.038	7124.47	CoI(53)			14.34		
7125.752	7125.283	FeI(1220)	4.60−6.34	−1.465	32.71	0.468	35.65
7126.566	7126.19	CaI	6.02−7.77	−0.647	60.47	0.375	31.74
7419.082	7418.668	FeI(1001)	4.12−5.79	−1.17	107.8	0.414	32.62
7420.15	7419.31	NiI(287)	5.50−7.17	−0.695		0.839	49.84
7422.671	7422.30	NiI(139)	3.69−5.28	+0.06	57.36	0.371	30.88

Table 1. continued

λ obs (Å)	λ lab (Å)	ID	χ (eV)	log gf	$F_\lambda{}^*$ (mÅ)	$\Delta\lambda$ (Å)	$V_{\rm Helio}$ km s^{-1}
7430.991	7430.5	FeI(204)	2.58−4.24	−3.81	21.02	0.491	35.71
7432.698	7431.97	TiI(142)	1.74−3.41	−2.283	15.53	0.728	45.27
7435.814	7435.3	unid			47.41		
7437.521	7437.16	CoI(53)	1.95−3.61	−3.64	45.96	0.360	30.43
7440.984	7440.6	TiI(225)	2.25−3.90	−1.19	38.7	0.383	31.35
7446.188	7445.70	FeI(1077)	4.24−5.90	−0.31	61.72	0.487	35.53
7449.784	7449.34	FeII(73)	3.87−5.53	−3.60	316.5	0.444	33.77
7450.505	7450.33	YII(?)				0.174	22.92
7452.982	7452.50	FeII(14F)			54.88		
7462.061	7461.527	FeI(204)	2.55−4.20	−3.48		0.534	37.36
7462.889	7462.38	FeII(73)	3.87−5.53	−2.98	540.5	0.509	36.35
8327.273	8327.061	FeI(60)	2.20−3.69	−1.298	307.8	0.212	23.79
8330.807	8330.587	unid			55.59		
8332.142	8331.926	FeI(1153)	4.39−5.88	−1.020	36.98	0.215	23.89
8335.342	8335.150	CI(10)	7.70−9.19	−0.420	69.24	0.191	23.01
8339.584	8339.398	Fe(1153)	4.44−5.93	−1.421	51.58	0.185	22.80
8349.31	8349.02	FeI(12)	0.91−2.40	−5.605	106.4	0.290	26.54
8364.508	8364.243	TiI(33)	0.83−2.32	−1.652	28.96	0.264	25.61
8365.885	8365.642	FeI(623)	3.25−4.74	−2.040	110.0	0.243	24.84
8675.626	8674.751	FeI(339)	2.82−2.42	−1.89	100.7	0.875	46.10
8676.22	8675.38	TiI(68)	1.06−2.50	−1.357	43.2	0.839	44.88
8689.396	8688.632	FeI(60)	2.17−3.59	−1.41	393.9	0.764	42.24
8693.139	8692.34	TiI(68)	1.04−2.46	−1.92	27.48	0.798	43.41
8727.923	8727.4	[CI]			302.5	0.522	33.80
8735.521	8734.70	TiI(68)	1.05−2.48	−2.087		0.821	44.05

were noticed in other post-AGB supergiants (García-Lario et al. 1997; Hrivnak 1997).

5. Atmospheric parameters and chemical composition

The UV (IUE) low resolution spectrum of HD 101584 matches well with that of an A6Ia star (HD 97534) (Fig. 9) indicating a $T_{\rm eff}$ of 8400 K (Lang 1992). The presence of CII lines at 6578 Å and 6582 Å indicates a $T_{\rm eff} >$ 8000 K. For $T_{\rm eff} \leq$ 8000 K the CII lines would be very weak or absent. The Paschen lines also indicates a low gravity (Fig. 10). The luminosity class Ia also indicates a very low gravity. From the analysis of several nitrogen lines around 7440 Å and 8710 Å we derived the microturbulence velocity $V_{\rm turb}$ = 13 km s^{-1}. We synthesised the spectral region from 4000 Å to 4700 Å (Fig. 11) with low gravity (log g = 1.5) models of Kurucz (1993) with temperatures 8000 K, 8500 K and 9000 K. The best fit was found for $T_{\rm eff}$ = 8500 K, log g = 1.5, $V_{\rm T}$ = 13 km s^{-1} and [Fe/H] = 0.0.

The line at 5876 Å was identified as a HeI line by Bakker et al. (1996a) who also state that the lines at 5047 Å and 5045 Å as due to HeI and NII respectively. However, we find that the 5047 and 5045 lines are in fact due to FeII. Except HeI 5876 Å, we have not found any other helium lines in the spectrum and nor have we found any NII or OII lines. In fact, Hibbert et al. (1991) indicate the presence of a CI line at 5876 Å. It is likely that the line at 5876 Å may be due to CI instead of HeI.

If we assume that the 5876 Å line is due to HeI then for a solar helium abundance and log g = 1.5, $T_{\rm eff}$ = 9000 K is found. Since we do not see any other helium lines, if 5876 Å line is due to helium, it is likely that it may be formed in the stellar wind or in the chromosphere of the star. On the basis of the presence of this helium line Bakker et al. (1996a) suggested that HD 101584 is a B9II star of $T_{\rm eff}$ 12000 K. On the basis of the analysis of our spectra we have not found any evidence for such a high temperature. We have also analysed the equivalent widths of absorption lines in the spectrum of HD 101584 given by Bakker et al. (1996a). The final abundances of some of the elements are listed in Table 2. The abundances listed in Table 2 show that the star is overabundant in carbon and nitrogen. It appears that the material processed by the triple alpha C-N and O-N cycle has reached the surface.

6. Discussion and conclusions

The optical spectrum of the post-AGB star HD 101584 is rather complex. We find several emission lines and P-Cygni profiles indicating an ongoing mass-loss and the presence of a circumstellar gaseous envelope. From the analysis of the absorption lines we find the atmospheric

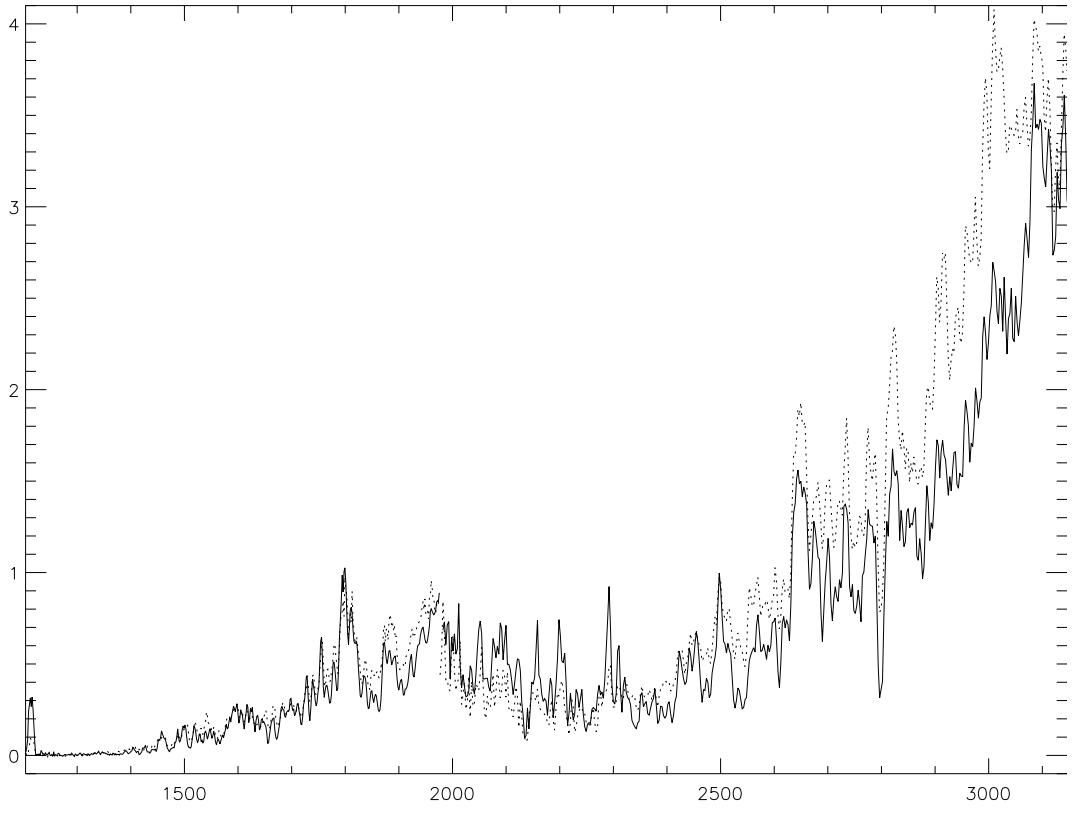

Fig. 9. IUE low resolution spectrum of HD 101584 is compared with that the A6Ia star HD 97534. The dotted line corresponds to the spectrum of HD 97534 while the solid line is HD 101584

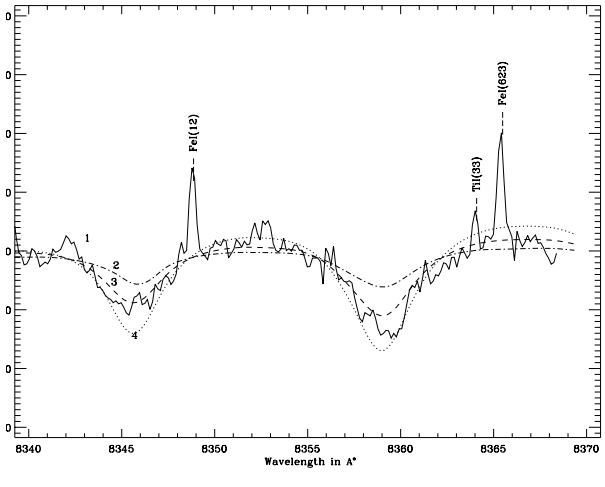

Fig. 10. Observed and synthetic spectra in the Paschen line region. 1-observed, 2-$T_{\rm eff}$ = 8000 K, log g = 1.0, 3-($T_{\rm eff}$ = 8000 K, log g = 2.0, 4-$T_{\rm eff}$ = 8500 K, log g = 1.5. The peaks are FeI emission lines

parameters to be $T_{\rm eff}$ = 8500 K, log g = 1.5, $V_{\rm t}$ = 13 km s^{-1} and [Fe/H] = 0.0.

Carbon and Nitrogen are found to be overabundant indicating that material processed by triple alpha C-N and O-N cycles has reached the surface. Since our blue spectra are of relatively low resolution and because of the presence of emission and shell components it is difficult to estimate reliable abundances of s-process elements. The OI line at 6156 Å is blended with a weak FeI emission line. The OI triplet at 7777 Å is very strong and affected by NLTE. In any case it appears that the oxygen abundance is nearly solar. A NLTE analysis of the high resolution OI 7777 Å triplet may yield a more reliable oxygen abundance.

The nitrogen abundance is based on 6 lines in the 7440 Å and 8710 Å region. We have not used the strong nitrogen lines. Nitrogen seems to be clearly overabundant. The carbon abundance is based on two CII lines at 6578 Å and 6582 Å. There is a clear indication that carbon is overabundant. The abundance of Mg, Ti, and Fe are nearly solar. The Ti abundance is based on 15 lines and the Fe abundance is based on 6 lines. Many of the other atomic lines are affected by emission and shell components. In our opinion, the line at 5876 Å might be due to CI (Hibbert et al. 1991) and not to HeI, as previously suggested by Bakker et al. (1996a). We have not found any other HeI, NII or OII lines. Our analysis shows that the $T_{\rm eff}$ is 8500 ± 500 K.

Bakker et al. (1996b) found small amplitude light and velocity variations and suggested that HD 101584 is a binary with an orbital period of 218 days. The radial velocity variations may be due to pulsation, macroturbulence motions or shock waves in the outer layers of the stellar atmosphere. Many post-AGB supergiants show small

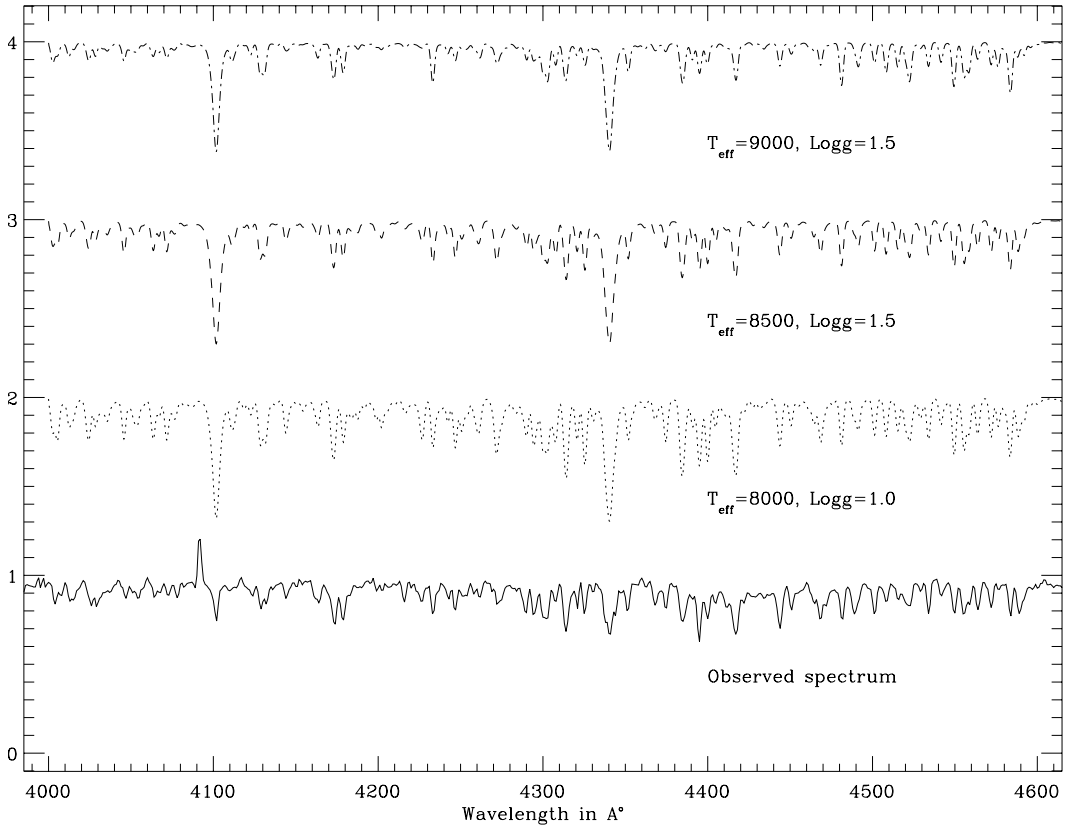

Fig. 11. Synthesis spectra for different models are compared with the observed spectrum. The observed spectrum is of 2.5 Å resolution taken at VBO kavalur. Observed spectrum matches well for $T_{\rm eff}$ = 8500 K, log g = 1.5, $V_{\rm turb}$ = 13 km s^{-1} and [Fe/H] = 0.0

Table 2. Chemical composition of HD 101584

Element	[element/H]		Lines
	$T_{\rm eff}$ = 8500 K log g = 1.5	$T_{\rm eff}$ = 9000 K log g = 1.5	
C	1.0 ± 0.1	0.3 ± 0.1	C II 6578, 6582
N	0.5 ± 0.1	0.6 ± 0.1	N I 7423, 7442, 8703, 8711, 8718, 8728
O	0.1	0.18	O I 6158
Mg[1]	0.2	0.02	Mg II 4481.13
Ti[1]	0.0 ± 0.4	0.4 ± 0.4	Ti II 15 lines
Fe[1]	−0.1 ± 0.1	0.5 ± 0.1	Fe I 3 lines
	0.2 ± 0.4	0.3 ± 0.4	Fe II 6lines

amplitude light and velocity variations (Hirvnak 1997). These variations may not be interpreted as due to the presence of a binary companion. Long term monitoring of the radial velocities is needed in order to understand the causes for these variations.

The spectrum and the brightness of HD 101584 appears to remain the same during last two or three decades. There is no evidence for significant variations in brightness similar to those observed in Luminous Blue Variables (LBVs). The chemical composition and all the available multiwavelength observational data collected during the last two decades by various observers indicates that HD 101584 is most likely a post-AGB star.

The presence of several P-Cygni lines with significant outflow velocities, the OH maser and CO emission profiles (Te Lintel Hekkert et al. 1992; Trams et al. 1990) and the IRAS infrared fluxes and colours (Parthasarathy & Pottasch 1986) indicates the possibility that HD 101584 is a post-AGB star with a bipolar outflow with a dusty disk. Since HD 101584 shows a strong Hα emission line, high resolution imaging with the Hubble Space Telescope (HST) may reveal the bipolar nebula and the presence of a dusty disk similar to that observed in other post-AGB stars like IRAS 17150-3224 (Kwok et al. 1998) or IRAS 17441-2411 (Su et al. 1998).

References

Bakker E.J., 1994, A&AS 103, 189
Bakker E.J., Lamers H.J.G.L.M., Waters L.B.F.M., Waelkens C., Trams N.R., Van Winckel H., 1996a, A&A 307, 869

Bakker E.J., Lamers H.J.G.L.M., Waters L.B.F.M., Waelkens C., 1996b, A&A 310, 861
Friedjung M., Muratorio G., 1987, A&A 188, 100
García-Lario P., Parthasarathy M., de Martino D., Monier R., Manchado A., de Córdoba S.F., Pottasch S.R., 1997, A&A 326, 1103
García-Lario P., Manchado A., Parthasarathy M., Pottasch S.R., 1994, A&A 285, 179
Hibbert A., Biémont E., Godefroid M., Vaeck N., 1991, A&AS 88, 505
Hrivnak B., 1997, in Planetary Nebulae, Habing H.J. and Lamers H.J.G.M. (eds.), IAU Symp. No. 180, 303
Hoffleit D., Saladya M., Wlasuk P., 1983, Supplement to the Bright star Catalogue, Yale University Observatory, U.S.A.
Hubeny I., Stefl S., Harmanec P., 1985, Bull. Astron. Inst. Czechosl. 36, 214
Humphreys R.M., 1976, ApJ 206, 122
Humphreys R.M., Ney E.P., 1974, ApJ 190, 339
Kurucz R.L., 1994, Solar Abundance Model Atmospheres, Kurucz CD-ROM No. 19, Smithsonian Astrophysical Observatory
Kwok S., Su K.Y.L., Hrivnak B.J., 1998, ApJ 501, L117
Lang K.R., 1992, Astrophysical data: Planets and stars. Springer Verlag
Morrison N.D., Zimba J.R., 1989, BAAS 21, 1022
Osterbrock D.E., 1989, Astrophysics of Gaseous Nebulae and Active Galactic Nuclei. Oxford University Press, p. 117
Parthasarathy M., García-Lario P., Pottasch S.R., 1992, A&A 264, 159
Parthasarathy M., Pottasch S.R., 1986, A&A 154, L16
Reddy B.E., Parthasarathy M., Gonzalez G., Bakker E.J., 1997, A&A 328, 331
Rosenzweig P., Reinoso E.G., Naranjo O., 1997, JRASC 91, 255
Su K.Y.L., Volk K., Kwok S., Hrivnak B.J., 1998, ApJ 508, 744
Te Lintel Hekkert P., Chapman J.M., Zijlstra A.A., 1992, ApJ 390, L23
Trams N.R., Van der Veen W.E.C.J., Waelkens C., Waters L.B.F.M., 1990, A&A 233, 153
Viotti R., 1969, Astrophys. Space Sci. 5, 323
Wiese W.L., Smith M.W., Glennon B.M., Atomic Transition Probabilities, Vol. 1, NSRDS-NBS(U.S.) 4, 1966
Wiese W.L., Martin G.A., Wavelength and Transition Probabilities for Atoms and Atomic Ions, NSRDS-NBS(U.S.) 68, 1980